Article

Discovery Medicine 2026; 38(206): 851–865
https://doi.org/10.24976/Discov.Med.202638206.70

EGR2 Targets Insulin Receptor Substrate 2 and Affects the Children's Type 1 Diabetes Progression *In Vivo* and *In Vitro*

Xiaofeng Sun[1,†], Jin Liu[1,†], Ji'ou Zhao[2], Gang Zhang[3], Wendi Zhou[1,*]

[1]Department of Pediatrics, The Affiliated Huaian No.1 People's Hospital of Nanjing Medical University, 223300 Huaian, Jiangsu, China
[2]College of Pediatrics, Nanjing Medical University, 211166 Nanjing, Jiangsu, China
[3]Department of Cardiology, The Affiliated Huaian No.1 People's Hospital of Nanjing Medical University, 223300 Huaian, Jiangsu, China
*Correspondence: wdzhou65734@163.com (Wendi Zhou)
[†]These authors contributed equally.
Submitted: 24 October 2025 Revised: 26 January 2026 Accepted: 13 February 2026 Published: 20 March 2026

Background: Early Growth Response 2 (EGR2) is a transcription factor implicated in inflammation and cell stress, yet its role in the pathogenesis of pediatric type 1 diabetes (T1D) remains largely unexplored. Moreover, the molecular mechanisms linking EGR2 to pancreatic β-cell dysfunction in T1D are unknown. This study aimed to elucidate the role of EGR2 in T1D progression and to explore the underlying molecular mechanisms.

Methods: The expression profile of dataset GSE9006 was analyzed using R software to assess EGR2 expression in peripheral blood mononuclear cells (PBMCs) from children with T1D. Bioinformatic analyses were further complemented by experimental validation to confirm these findings. The effects of EGR2 on MIN6 cell function were examined using Cell counting kit-8 (CCK-8) assay, 5-Ethynyl-2′-deoxyuridine (EdU) proliferation assay, flow cytometry, glucose-stimulated insulin secretion, quantitative PCR (qPCR), and immunoblotting. The regulatory influence of EGR2 on insulin receptor substrate 2 (IRS2) transcription was examined using qPCR and immunoblotting. *In vivo*, apoptosis was assessed by immunoblot analysis and Terminal deoxynucleotidyl transferase dUTP nick end labeling (TUNEL) assay, pancreatic islet injury was evaluated using hematoxylin and eosin (H&E) staining, and blood glucose levels were measured with a glucose meter.

Results: EGR2 is highly expressed in PBMC in children with T1D. In addition, EGR2 knockdown alleviated Cytomix-induced MIN6 cell dysfunction and inhibited IRS2 transcription. EGR2 knockdown ameliorated disturbances in STZ-induced blood glucose levels in mice, mitigated pancreatic islet injury in mice, and reduced apoptosis of mouse islet cells.

Conclusion: EGR2 knockdown enhances IRS2 transcription and mitigates the pathological features of T1D both *in vivo* and *in vitro*, suggesting that EGR2 may serve as a key regulator in T1D progression.

Keywords: EGR2; T1D; islet injury; IRS2; blood glucose

Introduction

Type 1 diabetes (T1D) is a progressive autoimmune disease caused by a combination of genetic and environmental factors [1]. The progression of T1D is characterized by insulin deficiency and the consequent loss of glucose homeostasis, which primarily results from the destruction of insulin-producing β-cells by β-cell–specific $CD8^+$ T cells [2]. Currently, insulin supplementation remains the cornerstone of therapy for both humans and experimental animals; however, no immunotherapeutic strategy has yet proven effective in preventing disease onset or halting the progression of T1D. As one of the most prevalent pediatric endocrine and metabolic disorders [3,4], T1D continues to impose a substantial health burden. Therefore, to improve clinical outcomes and therapeutic efficacy, it is essential to further elucidate its pathogenic mechanisms and identify more effective therapeutic targets.

Insulin receptor substrate (IRS) abnormalities are known to be associated with the development of insulin resistance, obesity, and diabetes mellitus (DM) [5]. Although IRS2-deficient mice are widely used to explore the pathophysiology of human type 2 diabetes, previous studies have also demonstrated that severe manifestations resembling T1D can occur in these mice, characterized by a marked elevation in blood glucose levels and the appearance of ketonuria [6]. Elevated IRS2 expression has been associated with improved insulin secretion and reduced β-cell death in human islets, suggesting that modulation of IRS2 may offer therapeutic benefit in T1D by preserving β-cell function and glucose homeostasis.

Early Growth Response 2 (EGR2) is a member of the early growth response gene family that contains three Cys2-His2 zinc finger domains that enable binding to conserved GC-rich DNA motifs, each consisting of approximately 28–

30 amino acids [7]. EGR2 is expressed across multiple tissues and cell types and plays a pivotal role in regulating inflammatory responses, apoptosis, and tissue injury [8]. Inhibition of EGR2 expression in cardiomyocytes has been shown to exert cardioprotective effects [9]. Furthermore, in type 2 diabetes, EGR2 expression is upregulated under insulin-resistant conditions, whereas EGR2 knockdown abolishes the effects of palmitic acid–induced insulin resistance in HepG2 cells, accelerates hepatic glucose uptake, and reverses lipid metabolic disturbances associated with insulin resistance [10]. However, the role of EGR2 in the T1D pathogenesis in children remains largely unexplored.

This study revealed significantly elevated EGR2 expression in the diabetic group via differential gene expression analyses of peripheral blood mononuclear cells (PBMCs) from children with T1D and healthy controls, based on the GSE9006 dataset. Further investigation revealed that EGR2 functions as a transcriptional factor regulating IRS2 expression. These findings demonstrate that EGR2 can serve as a potential therapeutic target for T1D in children.

Materials and Methods

Animals and Clinical Ethical Approval

The male C57BL/6 mice aged 8 weeks were obtained from VITAL RIVER Laboratory Animal Technology Co., Ltd. (Beijing, China). The protocols pertaining to animals were examined and authorized by the Animal Care and Use Committee of Nanjing Medical University (Approval No. KY-2023143). They were performed in accordance with international guidelines and institutional ethical policies regarding the use of laboratory animals.

All procedures involving human participants were performed in accordance with the standards of the Ethics Committee of the Affiliated Huaian No.1 People's Hospital of Nanjing Medical University (Approval No. KY-2022-021-01) and adhered to the principles outlined in the 1964 Helsinki Declaration and its subsequent amendments. Peripheral blood samples were collected from pediatric T1D patients (age range: 6–16 years) and age-matched healthy controls. Written informed consent was obtained from all legally authorized representatives (parents or guardians).

Peripheral blood mononuclear cells (PBMCs) were isolated from peripheral blood samples of 20 pediatric patients with newly diagnosed type 1 diabetes (T1D) and 20 age- and sex-matched healthy controls between January 2022 and December 2023. The inclusion criteria for T1D patients were: (1) diagnosis based on American Diabetes Association guidelines; (2) age at onset <18 years. Exclusion criteria included: (1) presence of other metabolic diseases; (2) recent infection or treatment with immunosuppressive therapy. Written informed consent was obtained from all legally authorized representatives (parents or guardians), and written assent was additionally obtained from children capable of comprehending the study, typically those aged ≥ 8 years.

Bioinformation Analysis

Microarray expression data were obtained from the Gene Expression Omnibus (GEO) database under accession number GSE9006. Differential gene expression analysis between pediatric T1D patients and healthy controls was performed using the Limma package in R software (version 4.2.2, R Foundation for Statistical Computing, Vienna, Austria). Genes with an absolute $\log_2$ fold change >1 and an adjusted p value < 0.05 were considered differentially expressed. Functional enrichment analyses, including Gene Ontology (GO) and Kyoto Encyclopedia of Genes and Genomes (KEGG) pathway analyses, were conducted using the DAVID database to explore the biological significance of the differentially expressed genes.

Animal Model Construction

A total of 32 male C57BL/6 mice were randomly assigned into four groups (n = 8 per group): Control (citrate buffer only), STZ, STZ + sh-NC, and STZ + sh-EGR2. The mice were divided into the indicated groups: STZ group: Diabetic mice without further treatment; STZ + sh-NC group: Diabetic mice receiving a tail-vein injection of lentivirus carrying a non-targeting short hairpin RNA (1×10^8 TU); STZ + sh-EGR2 group: Diabetic mice receiving a tail-vein injection of lentivirus carrying EGR2-targeting shRNA (1×10^8 TU). The above-detailed male C57BL/6 mice (20–25 g) were maintained in controlled, specified pathogen-free (SPF) environment of a 12-h dark/light cycle, relative humidity 55 $\pm$ 5%, and 22 $\pm$ 2 °C, with unrestricted availability of water and standard chow. To establish a diabetic model, mice were fasted overnight for 12 hours and then received intraperitoneal injections of freshly prepared STZ (S0130; Beyotime Biotechnology, Shanghai, China) at a dosage of 50 mg/kg body weight for five consecutive days. STZ was immediately dissolved in cold 0.1 M citrate buffer of pH 4.5 before use to maintain its stability. The criteria for a successful model are rigorously defined by the achievement of stable hyperglycemia (fasting blood glucose >11.1 mmol/L), the presence of characteristic pathological changes (such as pancreatic islet damage or insulin resistance), and the reproducibility of these features across the experimental cohort. Control mice were given an equivalent volume of citrate buffer alone. A glucose meter (Accu-Chek, Roche Diagnostics, Mannheim, Germany) was applied to measure fasting blood sugar from tails' vein blood on days 3, 7, and 14 after the final STZ injection. To minimize variability, all measurements were conducted in the morning following an overnight fast, and investigators responsible for data collection were blinded to group allocation. At the designated endpoints of the study, mice were humanely euthanized. The euthanasia procedure

was performed following an overnight fast to ensure standardized metabolic conditions. Sodium pentobarbital (150 mg/kg) was intraperitoneally injected into mice for anesthetization. Anesthesia depth was confirmed via the absence of both pedal and corneal reflexes. Once a surgical plane of anesthesia was achieved, terminal blood collection was performed via cardiac puncture from the left ventricle. Death was confirmed by exsanguination, along with the cessation of respiration and heartbeat.

Virus Infection

Recombinant lentiviruses encoding a scrambled negative control sequence (sh-NC) or a short-hairpin RNA (shRNA) targeting EGR2 (sh-EGR2) were purchased from GeneChem (Shanghai, China). These constructs were delivered using the GV248 vector, which includes a green fluorescent protein (GFP) reporter. The sequences were shown as follows: Sh-EGR2 AGAGAGCAGCGAUUGAUUAAU; Sh-NC UUCUCCGAACGUGUCACGU. For *in vitro* infection, MIN6 cells at 40–50% confluence were exposed to the respective lentiviruses at a multiplicity of infection (MOI) of 20 in 8 µg/mL polybrene for 12–16 h, followed by replacement with fresh culture medium. For *in vivo* transduction, mice received 1×10^8 TU of the respective lentivirus via tail-vein injection. The efficiency of infection was initially verified through GFP fluorescence imaging and subsequently confirmed by quantitative PCR and Western blot analyses of EGR2 expression levels.

Cell Culture

The mouse insulinoma MIN6 β-cell line (American Type Culture Collection, Manassas, VA, USA) was cultured in Dulbecco's Modified Eagle's Medium (DMEM, high glucose) supplemented with 10% fetal bovine serum (FBS), 100 U/mL penicillin, 100 µg/mL streptomycin, and 50 µM β-mercaptoethanol (M6250, Sigma-Aldrich, St. Louis, MO, USA). Cells were cultured in a humidified incubator at 37 °C with 5% CO_2. The culture medium was refreshed every 2–3 days. MIN6 cells were treated with a cytokine mixture (Cytomix), comprising recombinant mouse TNF-α (PeproTech, Rocky Hill, NJ, USA; 315-01A), IL-1β (PeproTech, Rocky Hill, NJ, USA; 211-11B), and IFN-γ (PeproTech, Rocky Hill, NJ, USA; 315-05-1MG), to stimulate an inflammatory environment. The Cytomix consisted of 10 ng/mL TNF-α, 5 ng/mL IL-1β, and 50 ng/mL IFN-γ. Cell cultures were tested for mycoplasma contamination using MycoAlert Mycoplasma Detection Kit (Lonza, Basel, Switzerland) to ensure they are free of mycoplasma.

MIN6 cells obtained from EK-Bioscience (CC-Y2103, Beijing, China) typically exhibit an epithelial-like morphology, forming polygonal or round cells with a high nucleus-to-cytoplasm ratio and a tendency to grow in compact monolayers or small clusters.

CCK-8 and 5-Ethynyl-2′-Deoxyuridine (EdU) Assay

For the CCK-8 assay, cells were seeded in 96-well plates at a density of 5×10^3 cells per well and allowed to adhere overnight, followed by incubation with the CCK-8 kit (C0038, Beyotime, China). After The absorbance at 450 nm was measured using a microplate reader (BioTek Synergy H1, Agilent BioTek, USA). Cell viability was calculated as a percentage relative to the control group: % Viability = (OD treatment – OD blank) / (OD control – OD blank) $\times$ 100%.

The proliferative capacity of MIN6 cells was evaluated by EdU incorporation assay. Briefly, coverslips in 24-well plates were used to seed 5×10^4 MIN6 cells at an appropriate density and treated according to the experimental design. After treatment, cells were incubated with 10 µM EdU (C0071S, Beyotime, China) at 37 °C for 2 h to incorporate into newly synthesized DNA. Cells was fixed at room temperature for 15 min with 4% paraformaldehyde and permeabilized for 10 min using 0.3% Triton X-100 in PBS. Incorporated EdU was detected using the Click-iT reaction mixture following the manufacturer's protocol, and nuclei were counterstained for 5 min with 1 µg/mL DAPI (C1002, Beyotime, Shanghai, China). Fluorescence images were captured using a Zeiss LSM 800 confocal microscope (Carl Zeiss, Germany), and representative fields were recorded for analysis.

Flow Cytometry Analysis of Apoptosis

Apoptosis of MIN6 cells was assessed using flow cytometry with an Annexin V-FITC/Propidium Iodide (PI) apoptosis detection kit according to the manufacturer's instructions (C1062L, Beyotime, China). Briefly, following the indicated treatments, cells were harvested, washed twice with cold PBS, and resuspended in binding buffer. Cells were then incubated with Annexin V-FITC and PI in the dark at room temperature for 15 min. Apoptotic cells were analyzed using a flow cytometer (BD FACSCanto II, BD Biosciences), and data were processed with FlowJo software (version 10.8.1; BD Biosciences, Ashland, OR, USA). Early apoptotic cells were defined as Annexin V-positive/PI-negative, while late apoptotic or necrotic cells were Annexin V-positive/PI-positive. The total apoptosis rate was calculated as the sum of early and late apoptotic populations. Flow cytometry data were analyzed using FlowJo software (version 10.8.1; BD Biosciences, Ashland, OR, USA).

Quantitative RT-PCR

Trizol (15596-026, Invitrogen, USA) was employed to isolate total RNA from both tissue samples and cultured cells, while PrimeScript RT Kit (RR037A, Takara, Japan) was used to synthesize cDNA according to the manufacturer's instructions. Quantitative RT-PCR was performed using SYBR Green Master Mix (Q111-02, Vazyme, China) on QuantStudio 3 machine (Applied Biosystems, USA).

The relative mRNA expression levels of target genes were calculated using the $2^{-\Delta\Delta Ct}$ method and normalized to the GAPDH gene. Primer sequences used were as follows: *EGR2*: Forward 5′-GCCAAGGCCGTAGACAAAATC-3′, Reverse 5′-CCACTCCGTTCATCTGGTCA-3′; *IRS2*: Forward 5′-ACCGACTTGGTCAGCGAAG-3′, Reverse 5′-CACGAGCCCGTAGTTGTCAT-3′; *GAPDH*: Forward 5′-AATGGATTTGGACGCATTGGT-3′, Reverse 5′-TTTGCACTGGTACGTGTTGAT-3′.

Western Blotting

RIPA lysis buffer (P0013B, Beyotime, Shanghai, China) with protease inhibitor cocktail (P8340, Sigma-Aldrich, USA) and phosphatase inhibitors (P1045, Beyotime) was employed to extract proteins from both cultured cells and pancreatic tissues. Lysates were incubated for 30 min on ice and centrifuged to remove insoluble debris at 4 °C for 15 min at 12,000 ×g. Protein concentrations were measured using BCA Protein Assay Kit (P0010, Beyotime). Equal amounts of proteins were separated by SDS-PAGE and then electrotransferred onto PVDF membrane (ISEQ00010, Millipore, USA). Membranes were blocked with 5% non-fat milk at room temperature for 60 min, followed by overnight incubation at 4 °C with the appropriate primary antibodies. The primary antibodies were obtained from Abcam (Cambridge, UK) and used at indicated working concentrations: anti-cleaved caspase-3 (ab214430, 1:1000), anti-Bcl-2 (ab182858, 1:1000), anti-Bax (ab182733, 1:1000), anti-IRS2 (ab134101, 1:1000), anti-Akt (ab8805, 1:1000), anti-p-Akt (ab38449, 1:1000), anti-EGR2 (ab108399, 1:1000), beta-actin (ab6276, 1:2000). Corresponding secondary antibodies (ab6721 & ab205719, 1:5000) were also obtained from Abcam and used to incubate membranes after washing according to the manufacturer's instructions, and visualized using an enhanced chemiluminescence (ECL) detection system (WBKLS0500, Millipore, USA). Signals were captured chemiluminescently using ChemiDoc XRS+ Imaging System (Bio-Rad, USA), and protein bands' relative intensities were determined using ImageJ software (version 1.53c; National Institutes of Health, Bethesda, MD, USA), normalized to GAPDH, and expressed as relative protein expression levels.

Immunofluorescence (IF) Staining

Pancreatic tissue slices were fixed using 4% paraformaldehyde and permeabilized using Triton X-100 (ST795, Beyotime, China) to allow antibody penetration. After permeabilization, tissue sections were blocked with 5% BSA to prevent non-specific bindings and, then incubated at 4 °C overnight with primary antibodies, including rabbit anti-insulin (ab181547, Abcam, Cambridge, UK; 1:200) and rabbit anti-glucagon (ab92517, Abcam, Cambridge, UK; 1:200). Secondary antibodies for IF analysis included goat anti-rabbit IgG H&L Alexa Fluor 488 (ab150077; 1:200), and goat anti-rabbit IgG H&L Alexa Fluor 594 (ab150080; 1:200). For detection of the macrophage marker F4/80, sequential staining was performed on separate sections or in a separate channel to avoid spectral overlap. Sections were incubated with the rat anti-F4/80 primary antibody, followed by goat anti-rat IgG H&L Alexa Fluor 594 to display F4/80 in red. Secondary antibodies were employed at a 1:500 dilution in PBS containing 1% BSA, and incubated for 1 h at room temperature in the dark. Afterward, cell nuclei were counterstained with DAPI (C1002, Beyotime, China) for nuclear visualization. Fluorescence images were acquired using a Zeiss LSM 800 microscope with consistent exposure settings for comparative analyses. Quantitative analysis of fluorescence intensity and protein band density was performed using ImageJ software (version 1.53c; National Institutes of Health, Bethesda, MD, USA).

Staining by Hematoxylin and Eosin (H&E)

HE staining was conducted on pancreatic tissue sections to evaluate tissue morphology. Paraffin-embedded sections were first deparaffinized in xylene (two changes, 10 minutes each), followed by rehydration through a graded ethanol series (100%, 95%, 80%, and 70%) and rinsing in distilled water. Sections were then stained with hematoxylin solution (H9627, Sigma-Aldrich, USA) for 5 min and rinsed under flowing tap water for 10 min. Differentiation was performed for 10 seconds using 1% acidic alcohol (1% HCl in 70% ethanol), followed by bluing in 0.2% aqueous ammonia for 30 seconds. Sections were counterstained with 0.5% eosin Y solution (E4009, Sigma-Aldrich, USA) for 2 min. The stained sections were then dehydrated through graded, cleared in xylene, and mounted with neutral resin (G8590, Solarbio, China). Histological morphology of pancreatic islets and surrounding tissues was examined using a light microscope (BX53, Olympus, Japan), and representative images were captured using a digital camera system (DP74, Olympus, Japan).

Enzyme-Linked Immunosorbent Assay (ELISA)

Blood was collected from mice via retro-orbital bleeding after an overnight fast (12 hours) to obtain serum, which was then separated by centrifugation at 3000 ×g for 15 min at 4 °C. Cell culture supernatants were collected at designated times for *in vitro* experiments and centrifuged at 1000 ×g for 5 min to remove debris. The samples were stored at –80 °C prior to analysis. Insulin concentration was measured using a mouse insulin ELISA kit (E-EL-M1382c, Elabscience, Wuhan, China) according to the manufacturer's instructions. In brief, a 50 µL sample or standard was added in duplicate to each well of a pre-coated 96-well plate and mixed with the horseradish peroxidase (HRP)-conjugated detection antibody. The plates were incubated at 37 °C for 30 min, washed five times with wash buffer, and then incubated in the dark at 37 °C for 15 min with 100 µL of tetram-

ethylbenzidine (TMB) substrate solution. The reaction was terminated by adding 50 µL stop solution (2 M H_2SO_4), and insulin levels were quantified by measuring optical density.

Chromatin Immunoprecipitation (ChIP) Assays

SimpleChIP Enzymatic Chromatin IP Kit (9003, Cell Signaling Technology, USA) was employed to conduct ChIP assays in accordance with the manufacturer's protocol. In brief, cells were cross-linked to preserve protein–DNA interactions, lysed, and subjected to sonication to shear chromatin into appropriate fragment sizes. Immunoprecipitation was performed using an anti-EGR2 antibody, with normal rabbit IgG (ab125938, Abcam; 1 µg per reaction) used as a negative control. Anti-EGR2 (ab108399) or normal IgG was used for the immunoprecipitation to pull down DNA–protein complexes. Precipitated DNA was subsequently purified and analyzed by qPCR to assess the *EGR2* binding to promoter regions of the *IRS2* gene.

Luciferase Reporter Assay

The IRS2 gene's promoter region containing the putative EGR2 binding site was cloned into the pGL3-basic luciferase vector (Promega, USA) to generate reporter constructs. Mutant constructs with altered EGR2 binding sequences were generated by site-directed mutagenesis to evaluate the specificity of EGR2 binding. IRS2 promoter constructs and EGR2 expression vector were employed using Lipofectamine 3000 (L3000008, Invitrogen, USA) to co-transfect MIN6 cells according to the manufacturer's instructions. Luciferase activity was measured using the Dual-Luciferase Reporter Assay (E1910, Promega, USA) after 48 hours of transfection, and recorded with a luminometer (GloMax, Promega, USA). Firefly luciferase activities were normalized to Renilla luciferase activities, and the results were expressed as relative luciferase activity. The pGL3-basic vector (E1751, Promega, USA). The sequence is shown as follows: E1: ACCCCGCACCCGCCT; E2: CTGCCACCCACAGCG; P1 WT: ACCCCGCACCCGCCT (–1661~–1675); P2 WT: CTGCCACCCACAGCG (–1507~–1521); P1 MUT: ACCCCTATATCGCCT. P2 MUT: CTGCCTGTGGTAGCG.

TUNEL Assay

Apoptotic cells in pancreatic tissue slices were detected using TUNEL apoptosis detection kit (C1086, Beyotime, China) according to the manufacturer's instructions. After labeling, all cells were visualized by counterstaining nuclei with DAPI, and fluorescence signals were explored using Zeiss LSM 800. The percent of TUNEL-positive cells to the total number of nuclei stained by DAPI was calculated in each field of view to quantify the apoptosis. Representative fluorescence images were captured under identical exposure conditions for comparative evaluation.

Autoimmune T1D Model Using NOD/LtJ Mice

Female NOD/LtJ mice (4 weeks old) were purchased from The Jackson Laboratory (Bar Harbor, ME, USA) and housed under specific pathogen-free (SPF) conditions (12 h light/dark cycle, 22 ± 2 °C, 55 ± 5% humidity) with free access to food and water. A total of 18 mice were randomly assigned into three groups (n = 6 per group): Control, sh-NC, and sh-EGR2.

At 6 weeks of age, mice in the sh-NC and sh-EGR2 groups received a single tail-vein injection of lentivirus carrying either non-targeting shRNA or EGR2-targeting shRNA (1×10^8 TU per mouse), while control mice received an equivalent volume of sterile PBS. Mice were monitored weekly for body weight and fasting blood glucose levels. The experimental duration continued for 8 weeks following viral administration.

At the study endpoint, mice were fasted overnight and euthanized by intraperitoneal injection of sodium pentobarbital (150 mg/kg). Adequate anesthesia was confirmed by the absence of pedal reflexes, followed by cardiac puncture for blood collection. Pancreatic tissues were rapidly excised, with portions fixed in 4% paraformaldehyde for histological, immunofluorescence, and TUNEL analyses, while the remaining tissues were snap-frozen in liquid nitrogen for protein extraction and Western blot analysis.

Statistical Analyses

The experimentations were independently performed in triplicate to ensure reproducibility, and quantitative data were provided as mean ± SD. GraphPad Prism 8.0 (San Diego, CA, USA) was employed for statistical analysis. For comparisons between two groups, an unpaired two-tailed Student's *t*-test was applied. Mann-Whitney U test was performed for comparisons between groups that do not meet the normal distribution. For comparisons among three or more groups, one-way ANOVA followed by Tukey's post hoc test was used. A p value < 0.05 was considered statistically significant.

Results

High EGR2 Expression in PBMCs From T1D Children

To investigate EGR2 expression profile in PBMCs from children with T1D, we analyzed transcriptomic data from the GSE9006 dataset. Differential gene expression was visualized using a volcano plot, which revealed that EGR2 was among the significantly upregulated genes in the diabetes group, with red points indicating genes with increased expression and grey points representing non-significant changes. As shown in Fig. 1A, the magnitude of upregulation suggested that EGR2 might be functionally associated with disease development. A heatmap comparing the expression of key genes between the diabetic and control groups further confirmed that EGR2,

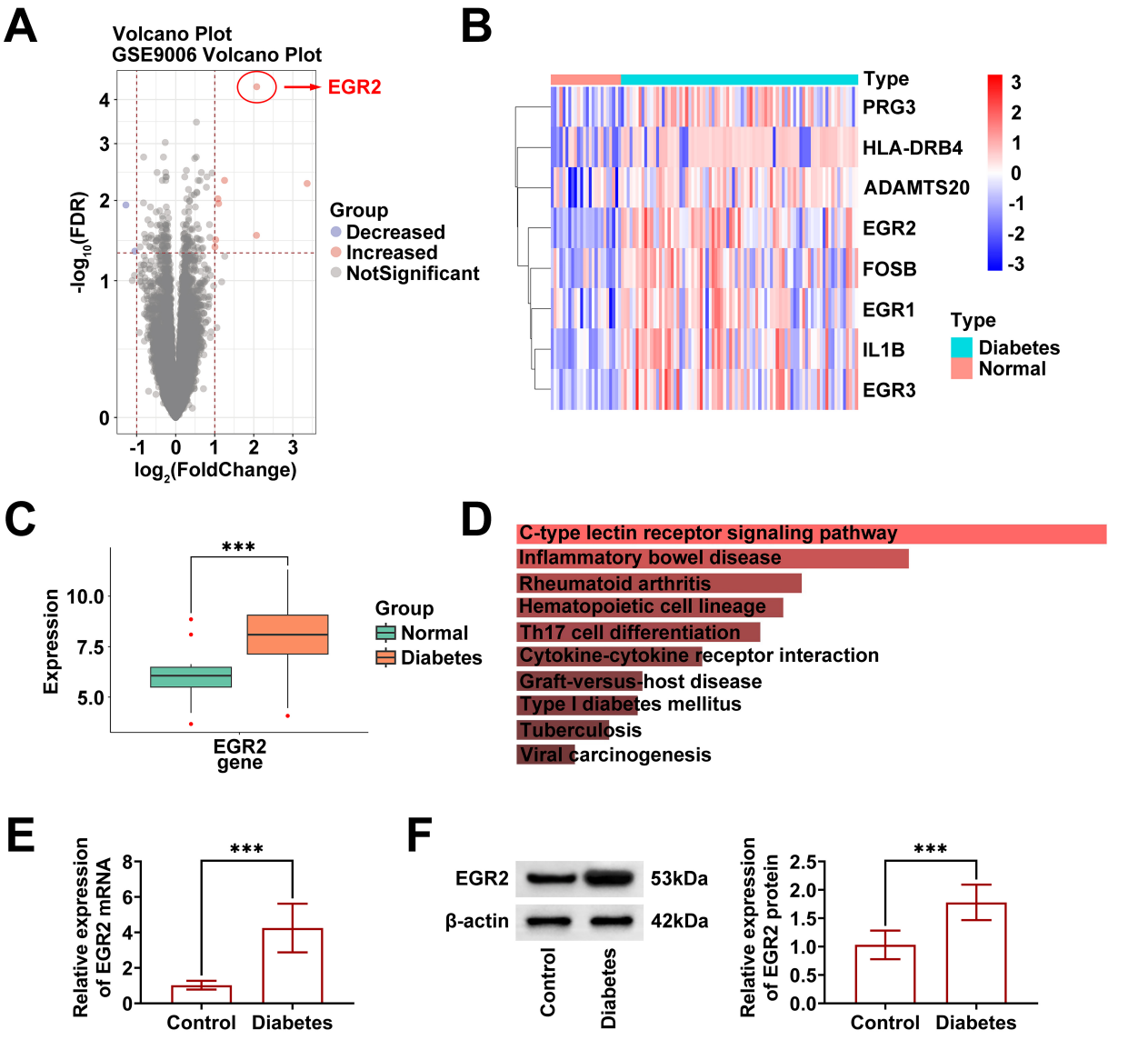

Fig. 1. High expression of EGR2 in PBMCs from type 1 diabetic (T1D) children. (A) Volcano plot illustrating differential gene expression in PBMCs of T1D children based on the GSE9006 dataset. Red points indicate significantly upregulated genes, while grey points represent non-significant changes. (B) Heatmap showing expression patterns of key genes in PBMCs from the diabetic and control groups, with red indicating higher expression and blue lower expression. (C) Box plot comparing EGR2 gene expression between the control and diabetes groups. 24 normal samples and 81 diabetic samples. ***$p < 0.001$ vs normal. (D) Pathway enrichment analysis highlighting immune-related pathways associated with genes upregulated in children with type 1 diabetes. (E) Quantitative RT-PCR showing EGR2 mRNA level in PBMCs from the control and diabetes groups. n = 20 in each group. (F) Western blotting of EGR2 protein expression in PBMCs; relative protein levels quantification is shown on the right. ***$p < 0.001$ vs control. EGR2, Early Growth Response 2; PBMCs, peripheral blood mononuclear cells.

along with several other genes, exhibited markedly higher expression levels in the diabetic group, as indicated by the red color gradient (Fig. 1B). Further analysis using a box plot analysis demonstrated that EGR2 gene expression was significantly elevated in PBMCs from children with T1D compared with those from healthy controls (***$p < 0.001$, Fig. 1C). Pathway enrichment analysis of the upregulated genes revealed several immune-related pathways, including cytokine–cytokine receptor interaction and C-type lectin receptor signaling pathway, highlighting the potential contribution of immune mechanisms to T1D pathogenesis (Fig. 1D). Experimental validation was then performed to confirm the bioinformatic findings. Quantitative RT-PCR analysis demonstrated significantly increased EGR2

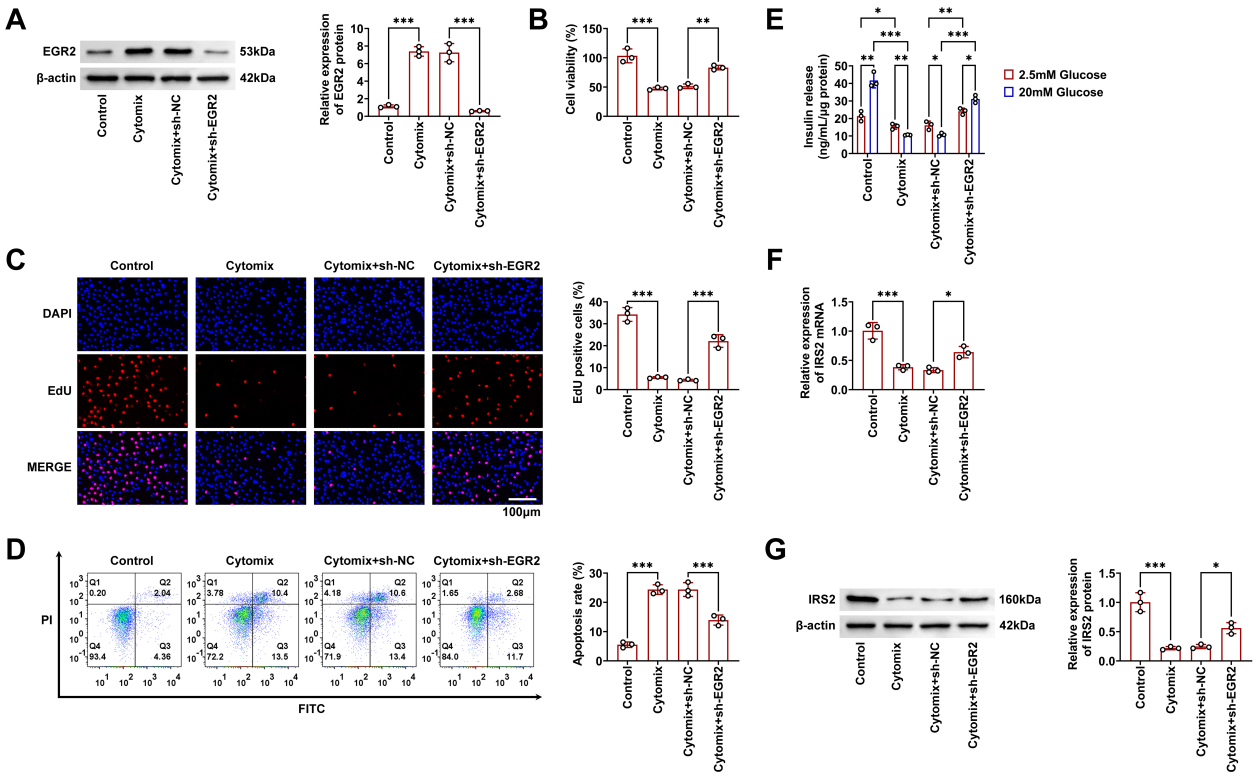

Fig. 2. EGR2 knockdown alleviates cytomix-induced functional impairment in MIN6 cells. (A) Western blotting showing EGR2 protein levels in the Control, Cytomix-treated, Cytomix + sh-NC (negative control for EGR2 knockdown), and Cytomix + sh-EGR2 (EGR2 knockdown) groups, with quantification of relative EGR2 expression presented on the right. The values are normalized to beta-actin as a loading control. (B) CCK-8 assays evaluating cell viability across the Control, Cytomix, Cytomix + sh-NC, and Cytomix + sh-EGR2 groups. (C) EdU incorporation assays assessing cell proliferation in the Control, Cytomix, Cytomix + sh-NC, and Cytomix + sh-EGR2 groups. Nuclei were counterstained with DAPI, and combined views are presented. Quantification of EdU-positive cells is provided on the right. Scale bar = 100 μm. (D) Flow cytometric analyses by PI (Propidium Iodide) and FITC (Fluorescein Isothiocyanate) staining to determine apoptosis rates in the Control, Cytomix, Cytomix + sh-NC, and Cytomix + sh-EGR2 groups, with quantitative results shown on the right. (E) ELISA (Enzyme-Linked Immunosorbent Assay) measuring insulin secretion in the Control, Cytomix, Cytomix + sh-NC, and Cytomix + sh-EGR2 groups under high (20 mM) and low (2.5 mM) sugar environments. (F) RT-PCR analyses of IRS2 mRNA expression in the Control, Cytomix, Cytomix + sh-NC, and Cytomix + sh-EGR2 groups. (G) Western blot analysis showing IRS2 protein levels in the Control, Cytomix, Cytomix + sh-NC, and Cytomix + sh-EGR2 groups, with quantification of relative IRS2 expression on the right. n = 3 in each group. *$p < 0.05$, **$p < 0.01$, ***$p < 0.001$.

mRNA expression in PBMCs from diabetics in comparison to healthy controls (***$p < 0.001$, Fig. 1E). Western blot analysis further confirmed elevated EGR2 protein levels in the diabetes group, and densitometric quantification exhibited significant enhancement in relative protein expression in comparison to controls (***$p < 0.001$, Fig. 1F). Collectively, these results indicate that EGR2 expression is markedly elevated at protein and mRNA levels in PBMCs of T1D children, demonstrating the potential function of EGR2 in mediating immune response involved in the disease process.

EGR2 Knockdown Alleviates Cytomix-Induced Functional Impairment in MIN6 Cells

To explore EGR2 function regarding pancreas β-cell physiology, we examined effects of EGR2 knockdown on Cytomix-induced dysfunction in MIN6 cells. Western blot analysis revealed a clear EGR2 elevation of protein expression in cells treated with Cytomix compared to untreated controls. In contrast, cells in the Cytomix + sh-EGR2 group depicted pronounced reduction of EGR2 protein levels, confirming effective knockdown (***$p < 0.001$, Fig. 2A). CCK-8 assay assessing cell viability exhibited that Cytomix treatment markedly decreased MIN6 cells' viability relative to controls. However, silencing of EGR2 in the Cytomix + sh-EGR2 group partially restored viability

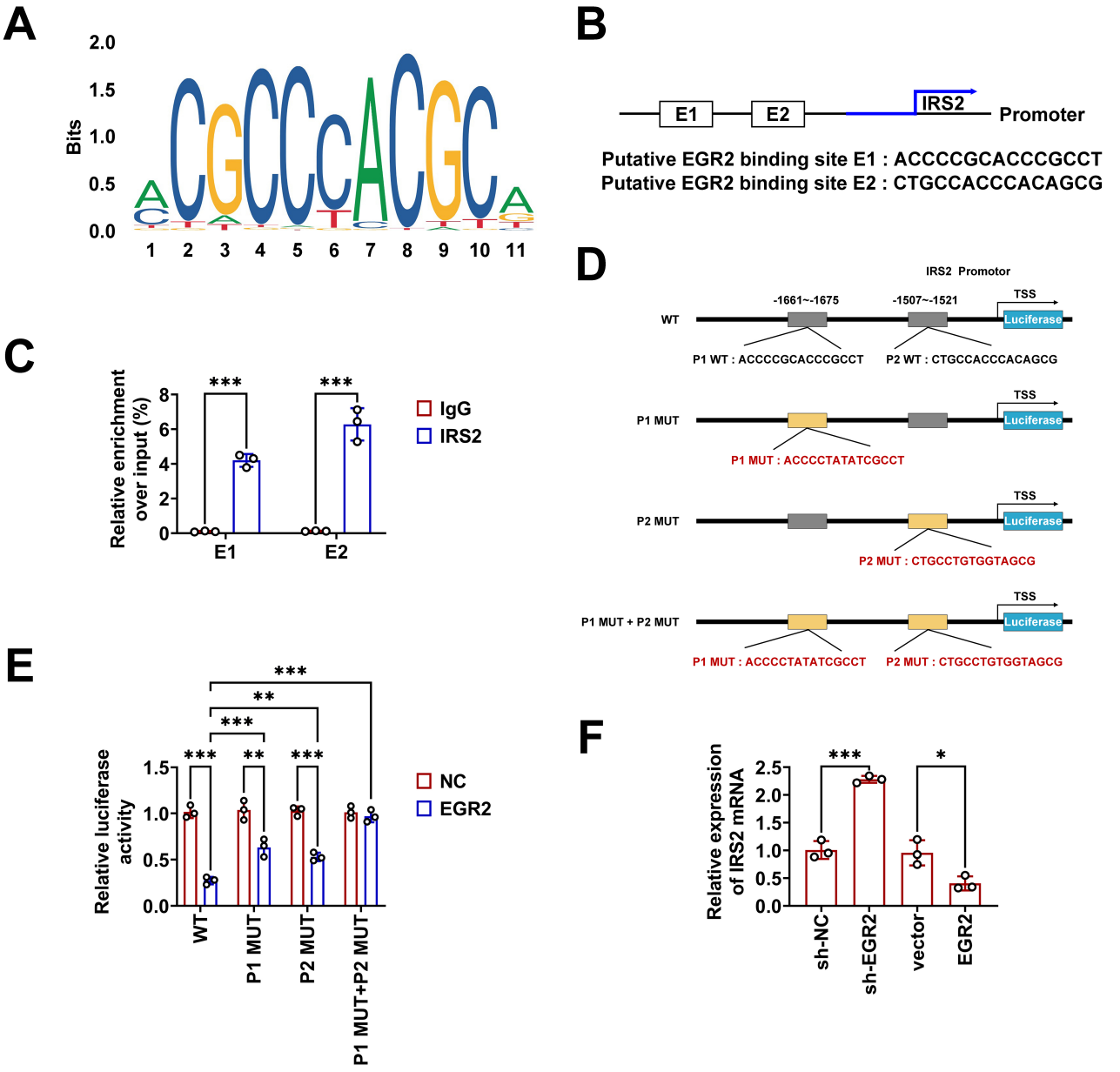

Fig. 3. EGR2 inhibits IRS2 transcription in STZ-induced mice. (A) Sequence logo representation of the putative EGR2 binding site motif. (B) Schematic diagram illustrating the IRS2 promoter region containing two predicted EGR2 binding sites, designated E1 and E2. (C) Chromatin immunoprecipitation (ChIP) assay showing the enrichment of EGR2 binding at the E1 and E2 sites in the IRS2 promoter region, with IgG employed as a negative control. (D) Schematics of wild-type (WT) and mutant (MUT) IRS2 promoter constructs used in luciferase reporter assays. P1 and P2 indicate the EGR2 binding sites, with mutations introduced in P1 MUT, P2 MUT, and P1 MUT + P2 MUT constructs. (E) Luciferase reporter assay showing relative luciferase activity in the WT and mutant (P1 MUT, P2 MUT, and P1 MUT + P2 MUT) IRS2 promoter constructs following EGR2 overexpression (EGR2) or negative control (NC) transfection. (F) Quantitative RT-PCR analysis showing IRS2 mRNA expression in the sh-NC, sh-EGR2 (EGR2 knockdown), vector control, and EGR2 overexpression groups. The values are normalized to GAPDH as a loading control. n = 3 in each group. *$p < 0.05$, **$p < 0.01$, ***$p < 0.001$.

when compared with both the Cytomix and Cytomix + sh-NC groups (**$p < 0.01$, Fig. 2B). Cell proliferation analysis using the EdU incorporation assay, with DAPI nuclear counterstaining, demonstrated that Cytomix exposure substantially decreased the number of EdU-positive cells, indicating suppressed proliferation. Conversely, EGR2 knockdown in the Cytomix + sh-EGR2 group resulted in a significant increase in EdU-positive cell counts, indicating

improved proliferative capacity (***$p < 0.001$, Fig. 2C). Apoptosis analysis by flow cytometry, using PI and FITC staining, revealed that Cytomix treatment significantly elevated apoptotic rates in MIN6 cells, while EGR2 knockdown effectively reduced the proportion of apoptotic cells in the Cytomix + sh-EGR2 group (***$p < 0.001$, Fig. 2D). To assess β-cell functional recovery, glucose-stimulated insulin secretion was analyzed using ELISA under both high (20 mM) and low (2.5 mM) glucose conditions. Cytomix treatment impaired insulin release, particularly under high glucose, whereas EGR2 silencing partially restored insulin secretion in the Cytomix + sh-EGR2 group (*$p < 0.05$, Fig. 2E). At the molecular level, qRT-PCR analysis revealed that Cytomix exposure significantly reduced IRS2 mRNA expression, while knockdown of EGR2 resulted in a substantial increase in IRS2 transcript level (*$p < 0.05$, Fig. 2F). Western blot analysis further corroborated these results, showing that IRS2 protein levels were decreased by Cytomix treatment but restored following EGR2 knockdown (*$p < 0.05$, Fig. 2G). Taken together, these findings demonstrate that EGR2 knockdown mitigates Cytomix-induced functional impairment in MIN6 cells by enhancing cell viability and proliferation, reducing apoptosis, improving glucose-stimulated insulin secretion, and elevating IRS2 expression, thereby supporting the protective role of EGR2 silencing in β-cell function under inflammatory stress.

EGR2 Inhibits IRS2 Transcription in STZ-Induced Mice

To further elucidate the regulatory impact of EGR2 on IRS2 transcription, we analyzed the IRS2 promoter sequence to identify potential EGR2 binding motifs. A sequence logo representing the putative EGR2 binding motif was generated, illustrating the conserved nucleotides that may be potentially recognized by EGR2 (Fig. 3A). Analysis of the IRS2 promoter revealed two predicted EGR2 binding sites, designated as E1 and E2 (Fig. 3B). ChIP assays were conducted to experimentally verify the interaction between EGR2 and the IRS2 promoter. Outcomes demonstrated that EGR2 binding at both E1 and E2 regions was significantly enriched relative to the IgG control, confirming a specific and direct interaction of EGR2 with the IRS2 promoter (***$p < 0.001$, Fig. 3C). To investigate the functional consequences of this binding, luciferase reporter constructs containing the wild-type (WT) IRS2 promoter or mutant variants with altered EGR2 binding sequences at E1 (P1 MUT), E2 (P2 MUT), or both sites (P1 MUT + P2 MUT) were generated (Fig. 3D). Luciferase reporter assays depicted that overexpression of EGR2 markedly suppressed luciferase activities in WT promoter construct, while mutations at either or both binding sites alleviated this repression (**$p < 0.01$, Fig. 3E). To further support these observations, quantitative RT-PCR analysis was conducted to assess IRS2 mRNA levels under various experimental conditions. In the sh-NC and vector control groups, IRS2 expression remained stable, whereas EGR2 knockdown (sh-EGR2) significantly increased IRS2 mRNA expression. Conversely, EGR2 overexpression resulted in a pronounced decrease in IRS2 transcript levels, reinforcing the conclusion that EGR2 functions as a transcriptional repressor of IRS2 (*$p < 0.05$, Fig. 3F). Together, these results demonstrate that EGR2 has direct binding with E1 and E2 portions of the IRS2 promoter and suppresses its transcriptional activity, thereby negatively regulating IRS2 expression.

EGR2 Knockdown Improves Blood Glucose Dysregulation in Mice Induced With STZ

To determine the *in vivo* significance of EGR2 in regulating glucose metabolism, EGR2 knockdown effects were examined on blood sugar homeostasis in diabetic mice induced with STZ. Western blotting revealed that EGR2 protein expression levels were markedly increased in pancreatic tissues from the STZ-treated group compared to control, while EGR2 expression was substantially reduced following lentiviral knockdown in the STZ + sh-EGR2 group. In contrast, IRS2 protein levels were decreased in the STZ-treated mice but were restored upon EGR2 knockdown, indicating an inverse relationship between EGR2 and IRS2 expression (***$p < 0.001$, Fig. 4A). Assessment of fasting blood glucose levels demonstrated that the STZ and STZ + sh-NC groups exhibited persistently higher glucose levels than controls, whereas the STZ + sh-EGR2 group showed a marked decrease in blood glucose concentrations (***$p < 0.001$, Fig. 4B). Similarly, serum insulin levels, reflective of pancreatic functional capacity, were significantly reduced in the STZ and STZ + sh-NC groups but were partially restored following EGR2 knockdown (*$p < 0.05$, Fig. 4C). The intraperitoneal glucose tolerance test (IPGTT) further revealed that severely impaired glucose tolerance was observed in the STZ and STZ + sh-NC groups; however, EGR2 knockdown in the STZ + sh-EGR2 group led to a notable improvement in glucose tolerance (***$p < 0.001$, Fig. 4D). Together, these findings indicate that EGR2 silencing ameliorates glucose dysregulation and improves pancreatic function in STZ-induced diabetic mice.

EGR2 Knockdown Reduces Islet Damage in STZ-Induced Mice

To evaluate whether EGR2 knockdown can mitigate pancreatic islet injury in STZ-induced diabetic mice, histological and IF analyses were performed on pancreatic tissue sections from the different experimental groups. HE staining revealed marked structural disruption and islet damage in both the STZ-treated and STZ + sh-NC groups compared to controls. Contrarily, EGR2 knockdown in the STZ + sh-EGR2 group notably preserved islet morphology and reduced histological evidence of tissue damage (Fig. 5A). IF staining for insulin (green) and glucagon (red)

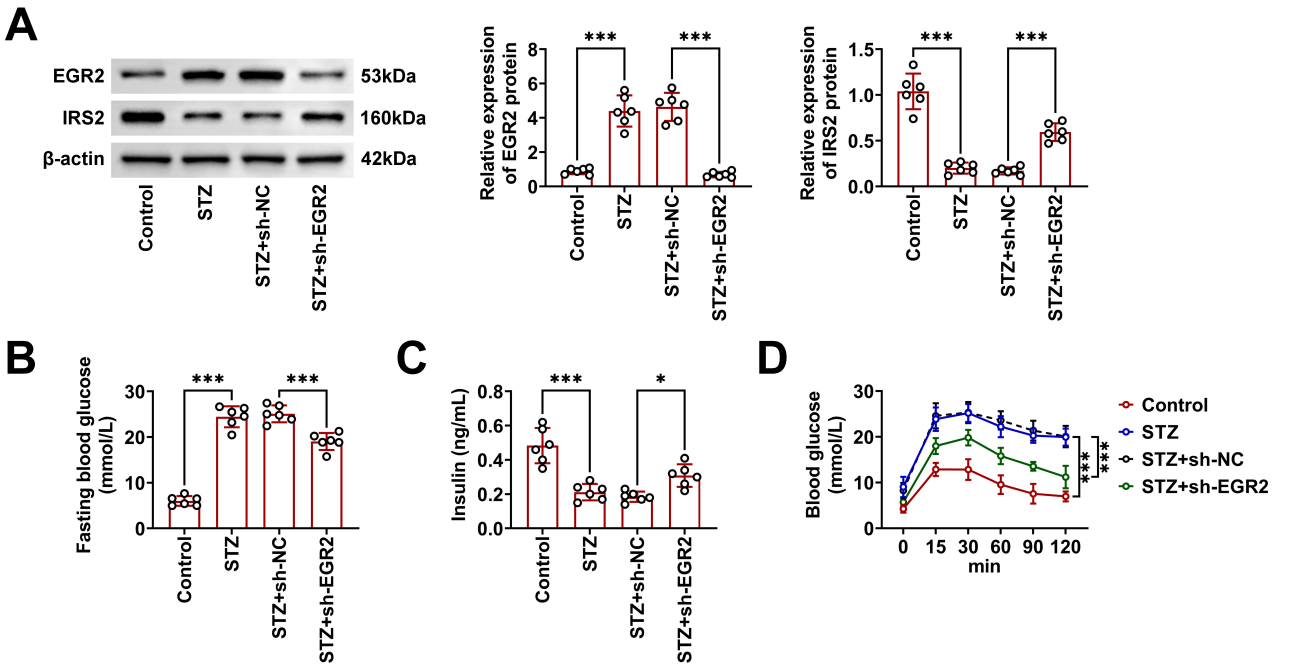

Fig. 4. EGR2 knockdown improves blood glucose dysregulation in mice induced with STZ. (A) Western blotting showing EGR2 and IRS2 protein levels in the Control, STZ-treated, STZ + sh-NC (negative control for EGR2 knockdown), and STZ + sh-EGR2 (EGR2 knockdown) groups. Quantification of relative protein expression for both EGR2 and IRS2 is presented on the right. (B) Fasting blood glucose levels in the Control, STZ, STZ + sh-NC, and STZ + sh-EGR2 groups. (C) Serum insulin concentrations measured in the Control, STZ, STZ + sh-NC, and STZ + sh-EGR2 groups. (D) Blood glucose recorded periodically in the intraperitoneal glucose tolerance test (IPGTT) in the Control, STZ, STZ + sh-NC, and STZ + sh-EGR2 groups. n = 6 in each group. $*p < 0.05$, $***p < 0.001$.

provided additional insights into islet cell function. In the STZ and STZ + sh-NC groups, insulin fluorescence intensity was markedly reduced, whereas glucagon fluorescence was increased, reflecting β-cell dysfunction and altered α-cell activity. Conversely, the STZ + sh-EGR2 group displayed enhanced insulin (red) fluorescence and decreased glucagon (green) fluorescence, suggesting improved preservation of both insulin- and glucagon-secreting cells ($**p < 0.01$, Fig. 5B). To further assess the inflammatory response associated with islet injury, macrophage infiltration was examined using F4/80 (red) IF staining. The STZ and STZ + sh-NC groups exhibited strong F4/80 fluorescence intensity, indicating pronounced macrophage infiltration within pancreatic tissues. In contrast, the STZ + sh-EGR2 group showed significantly weaker F4/80 fluorescence signals, suggesting attenuated macrophage infiltration and a reduction in local inflammatory activity ($***p < 0.001$, Fig. 5C). Collectively, these observations demonstrate that EGR2 knockdown effectively alleviates pancreatic islet damage and suppresses inflammation in STZ-induced diabetic mice.

EGR2 Knockdown Mitigates Islet Cell Apoptosis in STZ-Induced Mice

Apoptotic activity within pancreatic tissues was assessed using the TUNEL assay. The STZ and STZ + sh-NC groups displayed a high proportion of TUNEL-positive nuclei, indicating substantial enhancement in apoptosis of islet cell. In contrast, the STZ + sh-EGR2 group exhibited a substantially lower percentage of TUNEL-positive cells, suggesting that EGR2 knockdown effectively reduces apoptosis in pancreatic islet cells ($***p < 0.001$, Fig. 6A). Western blotting was conducted to evaluate the protein expression levels related to apoptosis, including cleaved caspase-3, Bcl-2, and Bax, which verified these outcomes at the molecular level. The STZ and STZ + sh-NC groups demonstrated elevated expression levels of cleaved caspase-3 and pro-apoptotic Bax, accompanied by a marked decrease in anti-apoptotic Bcl-2 proteins. However, EGR2 knockdown in the STZ + sh-EGR2 group reversed these alterations, leading to reduced cleaved caspase-3 and Bax and enhanced Bcl-2 expression ($***p < 0.001$, Fig. 6B).

We employed NOD/LtJ mice, a spontaneous T1D model characterized by progressive insulitis. H&E staining revealed extensive lymphocytic infiltration and severe islet destruction in both the Control and sh-NC groups, whereas EGR2 silencing markedly reduced immune cell infiltration and preserved islet structure (**Supplementary Fig. 1A**). Consistently, TUNEL analysis showed a high proportion of apoptotic β-cells in the sh-NC group, while the sh-EGR2 group exhibited a significantly lower apoptosis rate, indicating that EGR2 knockdown mitigates autoimmune-

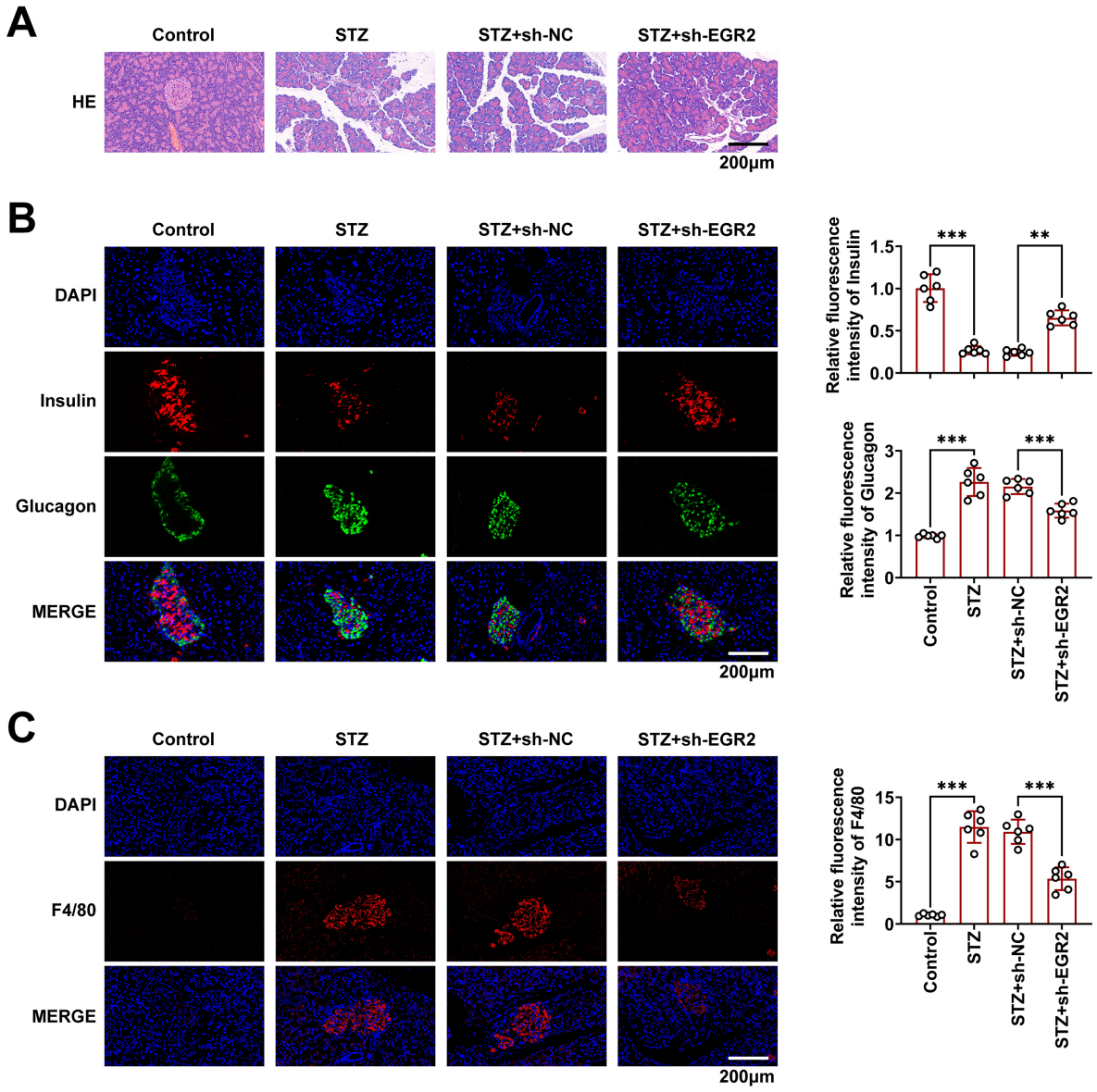

Fig. 5. EGR2 knockdown reduces islet damage in STZ-induced mice. (A) Staining by HE of pancreatic tissue slices of the Control, STZ-treated, STZ + sh-NC (negative control for EGR2 knockdown), and STZ + sh-EGR2 (EGR2 knockdown) groups. Scale bar = 200 μm. (B) Immunofluorescent staining of pancreas slices showing insulin (red) and glucagon (green) expression in the Control, STZ, STZ + sh-NC, and STZ + sh-EGR2 groups. DAPI was employed to counterstain nuclei. Quantification of relative fluorescence intensity for insulin and glucagon is presented on the right. The fluorescence intensity was quantified as the mean intensity per islet area using ImageJ software (version 1.53c; National Institutes of Health, Bethesda, MD, USA). Scale bar = 200 μm. (C) Immunofluorescent staining for F4/80 (red) to assess macrophage infiltration in pancreatic tissue of the Control, STZ, STZ + sh-NC, and STZ + sh-EGR2 groups. Nuclei were stained with DAPI. Quantification of relative fluorescence intensity for F4/80 is indicated on the right. Scale bar = 200 μm. n = 6 in each group. $^{**}p < 0.01$, $^{***}p < 0.001$.

mediated β-cell loss (**Supplementary Fig. 1B**). At the molecular level, Western blotting demonstrated that EGR2 deficiency robustly restored IRS2 protein expression and increased Akt phosphorylation relative to sh-NC, supporting reactivation of the IRS2–Akt survival pathway in β-cells (**Supplementary Fig. 1C**).

In summary, these results indicate that EGR2 knockdown mitigates islet cell apoptosis in STZ-induced diabetic mice by modulating apoptosis-associated protein expression.

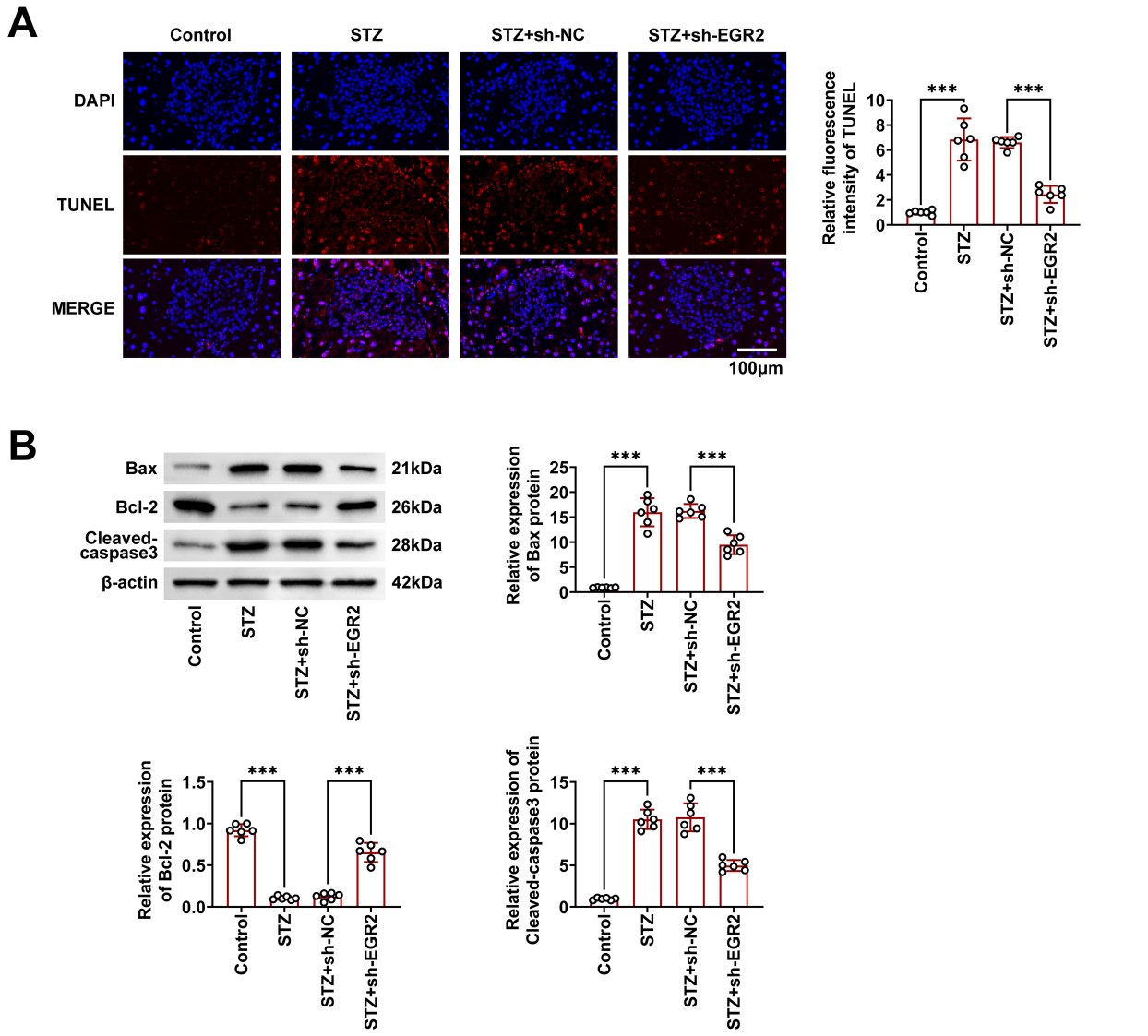

Fig. 6. EGR2 knockdown mitigates islet cell apoptosis in STZ-induced mice. (A) TUNEL assays detecting apoptosis cells in pancreatic tissue slices from the Control, STZ-treated, STZ + sh-NC (negative control for EGR2 knockdown), and STZ + sh-EGR2 (EGR2 knockdown) groups. DAPI was used for nuclear counterstaining, and merged pictures are shown. Quantification of relative apoptotic rate, expressed as the percentage of TUNEL-positive cells, is presented on the right. Scale bar = 100 μm. (B) Western blotting of proteins related to apoptosis, i.e., cleaved-caspase 3, Bcl-2, and Bax in the Control, STZ, STZ + sh-NC, and STZ + sh-EGR2 groups, with quantification of relative protein expression shown on the right. n = 6 in each group. ***$p < 0.001$.

Discussion

T1D is a chronic autoimmune disorder that mainly manifests during childhood and is characterized by the targeted destruction of pancreatic β-cells by the host immune system, resulting in an absolute deficiency of insulin and leading to persistent hyperglycemia [11]. Despite considerable progress in immunotherapeutic approaches, current treatment strategies remain insufficient to halt the progressive loss of β-cell function or to restore β-cell mass once it has been destroyed. This limitation emphasizes the need for a deeper understanding of T1D pathogenesis, particularly the molecular mechanisms driving β-cell dysfunction and immune-mediated cytotoxicity [12]. Since pancreatic β-cell integrity and function are essential for maintaining glucose homeostasis, preserving or restoring them represents a crucial strategy to improve disease outcomes. Contextually, the study herein elucidates the molecular interaction of EGR2 with IRS2 in β-cell regulation and T1D progression, thereby identifying potential therapeutic targets that may contribute to β-cell preservation and improved management of T1D.

The STZ-induced diabetic mouse model, which reproduces key pathological features of human T1D such as pancreatic β-cell destruction and persistent hyperglycemia, provides a valuable experimental platform for elucidating disease mechanisms and evaluating potential therapeutic interventions [13,14]. In current work, this model was employed for examining EGR2 knockdown impact on diabetes-related metabolic and inflammatory alterations. Our findings demonstrate that suppression of EGR2 expression in STZ-treated mice effectively ameliorated hyperglycemia, improved glucose tolerance, and preserved the structural and functional integrity of pancreatic islets. These results not only confirm the reliability of the STZ model in simulating T1D pathology but also substantiate its utility in investigating the protective effects of EGR2 inhibition and its downstream regulatory pathways.

EGR2, a member of the early growth response transcription factor family, participates in multiple cellular processes, including cell differentiation, immune regulation, and inflammatory responses [15–17]. Increasing evidence indicates that EGR2 also contributes to the regulation of metabolic and inflammatory pathways, suggesting its potential relevance to endocrine disorders [9,18]. In our study, expression of EGR2 was substantially enhanced in pancreatic tissues of STZ-induced diabetic mice, suggesting its involvement in the inflammatory and apoptotic responses associated with T1D pathogenesis. Notably, EGR2 knockdown resulted in decreased inflammation responses and reduced apoptosis within pancreatic islets, indicating that suppression of EGR2 confers protection against β-cell damage. These findings support the notion that EGR2 functions as a regulator of metabolic inflammation and can act as a promising therapeutic target for endocrine and metabolic disorders characterized by immune-mediated β-cell injury.

IRS, particularly IRS2, represents essential mediators of insulin signaling and plays critical roles in maintaining β-cell function and systemic glucose homeostasis. In the context of T1D, disruption of IRS-dependent signaling pathways contributes to insulin resistance, β-cell dysfunction, and acceleration of disease progression [10,19]. Among these substrates, IRS2 has been specifically associated with β-cell survival and the adaptive response to metabolic stress [20]. Consequently, targeting IRS and IRS2 signaling has been proposed as an approach to preserve β-cell function and improve insulin sensitivity in diabetes [4,21]. Consistent with this concept, our study revealed that EGR2 knockdown restored IRS2 expression under diabetic conditions, thereby enhancing insulin signaling and promoting β-cell survival. Collectively, these observations suggest that regulation of the EGR2–IRS2 axis may represent a possible therapeutic approach for preserving β-cell functions and improving metabolic control in T1D.

In vitro experiments using MIN6 cells, a well-established pancreatic β-cell model, further corroborated the *in vivo* observations obtained from the STZ-induced diabetic mouse model [22]. *In vitro* assays across in different cellular models further confirmed the role of EGR2 [23,24]. Our *in vivo* data demonstrate that EGR2 knockdown attenuates macrophage infiltration into pancreatic islets. Although direct mechanistic evidence was not established, this observation raises the possibility that EGR2 may regulate the production of key chemokines by β-cells that recruit macrophages, or may directly influence macrophage activation and polarization within the diabetic microenvironment.

Mechanistic analyses conducted in this study revealed that EGR2 directly regulates IRS2 transcription by binding to the IRS2 promoter region. Evidence from ChIP assays confirmed the physical interaction between EGR2 and the IRS2 promoter, while luciferase reporter assays demonstrated that EGR2 suppresses IRS2 promoter activity, thereby inhibiting its transcription. Through this mechanism, EGR2 exerts a downstream influence on insulin signaling and β-cell function. This novel transcriptional regulatory relationship between EGR2 and IRS2 introduces an additional level of control over insulin signaling pathways, suggesting that modulation of EGR2 activity could provide a targeted strategy for diabetes intervention.

The regulatory interplay between EGR2 and IRS2 suggests the broader impact of EGR2 on metabolic and inflammatory networks relevant to diabetes pathophysiology [10]. By downregulating IRS2 expression, EGR2 may influence both insulin sensitivity and glucose homeostasis, thereby contributing to β-cell dysfunction and metabolic dysregulation in T1D. Conversely, suppression of EGR2 enhances IRS2 transcription, improves β-cell resilience, and supports glucose regulation. Collectively, the outcomes herein reflect that modulation of the EGR2–IRS2 axis denotes a promising therapeutic approach to preserve β-cell function and maintain metabolic stability in T1D. A potential discrepancy in EGR2 expression between PBMCs and pancreatic islets could exist, where elevated EGR2 in PBMCs may signify a heightened systemic inflammatory state, while its upregulation within β-cells might reflect a direct response to local stress, leading to intrinsic dysfunction. Consequently, a therapeutic strategy targeting EGR2 could exert a dual benefit: systemically modulating the immune response and locally preserving β-cell function, thereby enhancing its potential applicability for T1D treatment.

Multiple limitations of the study herein must be acknowledged while the outcomes are being interpreted. The STZ-induced diabetes model, although widely used and reliable for inducing pancreatic β-cell destruction and hyperglycemia, represents a chemically mediated form of injury rather than the gradual, T-cell-driven autoimmune process characteristic of human T1D, particularly in children. Thus, while our findings demonstrate that EGR2 knockdown protects β-cells from STZ-induced apoptosis and functional impairment, the model herein may not completely encom-

pass immunopathological complexities of autoimmune β-cell loss. The absence of autoreactive lymphocyte infiltration in the STZ model further limits the ability to assess immune–β-cell interactions; therefore, conclusions regarding immunoregulatory mechanisms should be interpreted with caution. In addition, this study transitions from the identification of EGR2 upregulation in PBMCs of children with T1D to mechanistic investigations primarily focused on β-cell-intrinsic pathways. Although these findings establish a clear role for EGR2 in β-cell dysfunction, the potential immunological functions of EGR2 within immune cell populations, the central driver of T1D pathogenesis, remain unexplored. Future studies should examine whether EGR2 contributes to immune activation, macrophage recruitment, or other inflammatory processes that mediate β-cell destruction. Moreover, validation of these findings in autoimmune models like non-obese diabetic (NOD) mice, alongside assessment of EGR2 expression in human pancreatic islet tissue, would be necessary to determine the clinical and translational importance of targeting the EGR2–IRS2 axis in T1D.

Future studies employing autoimmune models, such as the NOD mouse, will be essential to determine whether EGR2 knockdown similarly preserves β-cell mass and function in the setting of T-cell-mediated autoimmunity, and to explore its role in regulating immune cell infiltration and activation within pancreatic islets. Furthermore, while our data establish EGR2 as a direct transcriptional repressor of IRS2, the upstream signals responsible for EGR2 induction in T1D remain to be fully elucidated. It is plausible that pro-inflammatory cytokines prevalent in the islet microenvironment, such as IL-1β, TNF-α, and IFN-γ, or cellular stress pathways activated during β-cell dysfunction, serve as key triggers for EGR2 upregulation. Future studies aimed at elucidating these upstream mechanisms will provide a more comprehensive understanding of the pathological cascade and could identify nodal points for therapeutic intervention.

Conclusion

In conclusion, our study demonstrates that EGR2 knockdown enhances IRS2 expression, reduces β-cell apoptosis, and improves glucose regulation in T1D models. These findings indicate that the EGR2–IRS2 axis plays a key role in T1D progression and β-cell survival, providing a possible therapeutic target to manage the disease.

Availability of Data and Materials

The datasets used and/or analyzed during the present study are available from the corresponding author on reasonable request.

Author Contributions

All authors contributed to the study conception and design. Material preparation and the experiments were performed by XS and JL. Data collection and analysis were performed by JZ and GZ. The first draft of the manuscript was written by WZ and all authors contributed to important editorial changes in the manuscript. All authors read and approved the final manuscript. All authors have participated sufficiently in the work to take public responsibility for appropriate portions of the content and agreed to be accountable for all aspects of the work in ensuring that questions related to its accuracy or integrity.

Ethics Approval and Consent to Participate

All procedures involving human participants were performed in accordance with the standards of the Ethics Committee of the Affiliated Huaian No.1 People's Hospital of Nanjing Medical University (Approval No. KY-2022-021-01), and adhered to principles outlined in the 1964 Helsinki Declaration and its subsequent amendments. All animal experiments were approved by the Animal Care and Use Committee of Nanjing Medical University (Approval No. KY-2023143) and conducted in accordance with the National Institutes of Health Laboratory Animal Care and Use Guidelines. The animal experiment complies with the ARRIVE guidelines and is in accordance with the National Institutes of Health guide for the care and use of Laboratory animals.

Acknowledgment

Not applicable.

Funding

This research received no external funding.

Conflict of Interest

The authors declare no conflict of interest.

Supplementary Material

Supplementary material associated with this article can be found, in the online version, at https://doi.org/10.24976/Discov.Med.202638206.70.

References

[1] Quattrin T, Mastrandrea LD, Walker LSK. Type 1 diabetes. Lancet (London, England). 2023; 401: 2149–2162. https://doi.org/10.1016/S0140-6736(23)00223-4.

[2] Ramos EL, Dayan CM, Chatenoud L, Sumnik Z, Simmons KM, Szypowska A, *et al*. Teplizumab and β-Cell Function in Newly Diagnosed Type 1 Diabetes. The New England Journal

of Medicine. 2023; 389: 2151–2161. https://doi.org/10.1056/NEJMoa2308743.

[3] Fagundes RR, Zaldumbide A, Taylor CT. Role of hypoxia-inducible factor 1 in type 1 diabetes. Trends in Pharmacological Sciences. 2024; 45: 798–810. https://doi.org/10.1016/j.tips.2024.07.001.

[4] Sperling MA, Laffel LM. Current Management of Glycemia in Children with Type 1 Diabetes Mellitus. The New England Journal of Medicine. 2022; 386: 1155–1164. https://doi.org/10.1056/NEJMcp2112175.

[5] Gorgisen G, Aydin M, Mboma O, Gökyildirim MY, Chao CM. The Role of Insulin Receptor Substrate Proteins in Bronchopulmonary Dysplasia and Asthma: New Potential Perspectives. International Journal of Molecular Sciences. 2022; 23: 10113. https://doi.org/10.3390/ijms231710113.

[6] Louzada RA, Blandino-Rosano M, Flores S, Lubaczeuski C, Cui T, Sha W, *et al*. GHRH agonist MR-409 protects β-cells from streptozotocin-induced diabetes. Proceedings of the National Academy of Sciences of the United States of America. 2023; 120: e2209810120. https://doi.org/10.1073/pnas.2209810120.

[7] Joseph LJ, Le Beau MM, Jamieson GA, Jr, Acharya S, Shows TB, Rowley JD, *et al*. Molecular cloning, sequencing, and mapping of EGR2, a human early growth response gene encoding a protein with "zinc-binding finger" structure. Proceedings of the National Academy of Sciences of the United States of America. 1988; 85: 7164–7168. https://doi.org/10.1073/pnas.85.19.7164.

[8] Yang L, Li L, Chang P, Wei M, Chen J, Zhu C, *et al*. miR-25 Regulates Gastric Cancer Cell Growth and Apoptosis by Targeting EGR2. Frontiers in Genetics. 2021; 12: 690196. https://doi.org/10.3389/fgene.2021.690196.

[9] Hou X, Hu G, Wang H, Yang Y, Sun Q, Bai X. Inhibition of Egr2 Protects against TAC-induced Heart Failure in Mice by Suppressing Inflammation and Apoptosis Via Targeting Acot1 in Cardiomyocytes. Journal of Cardiovascular Translational Research. 2025; 18: 574–585. https://doi.org/10.1007/s12265-025-10602-5.

[10] Lu L, Ye X, Yao Q, Lu A, Zhao Z, Ding Y, *et al*. Egr2 enhances insulin resistance via JAK2/STAT3/SOCS-1 pathway in HepG2 cells treated with palmitate. General and Comparative Endocrinology. 2018; 260: 25–31. https://doi.org/10.1016/j.ygcen.2017.08.023.

[11] Bright C. Breaking through barriers for type 1 diabetes: introducing Breakthrough T1D. British Journal of Sports Medicine. 2025; 59: 1321–1322. https://doi.org/10.1136/bjsports-2025-110281.

[12] Bluestone JA, Buckner JH, Herold KC. Immunotherapy: Building a bridge to a cure for type 1 diabetes. Science (New York, N.Y.). 2021; 373: 510–516. https://doi.org/10.1126/science.abh1654.

[13] Shen Q, Zhong YT, Liu XX, Hu JN, Qi SM, Li K, *et al*. Platycodin D ameliorates hyperglycaemia and liver metabolic disturbance in HFD/STZ-induced type 2 diabetic mice. Food & Function. 2023; 14: 74–86. https://doi.org/10.1039/d2fo03308a.

[14] Amalan V, Vijayakumar N, Indumathi D, Ramakrishnan A. Antidiabetic and antihyperlipidemic activity of p-coumaric acid in diabetic rats, role of pancreatic GLUT 2: In vivo approach. Biomedicine & Pharmacotherapy = Biomedecine & Pharmacotherapie. 2016; 84: 230–236. https://doi.org/10.1016/j.biopha.2016.09.039.

[15] Song A, Yan R, Xiong W, Xiang H, Huang J, Jiang A, *et al*. Early growth response protein 2 promotes partial epithelial-mesenchymal transition by phosphorylating Smad3 during renal fibrosis. Translational Research: the Journal of Laboratory and Clinical Medicine. 2024; 271: 13–25. https://doi.org/10.1016/j.trsl.2024.04.005.

[16] Yue L, Yu HF, Yang ZQ, Tian XC, Zheng LW, Guo B. Egr2 mediates the differentiation of mouse uterine stromal cells responsiveness to HB-EGF during decidualization. Journal of Experimental Zoology. Part B, Molecular and Developmental Evolution. 2018; 330: 215–224. https://doi.org/10.1002/jez.b.22807.

[17] Li W, He S, Tan J, Li N, Zhao C, Wang X, *et al*. Transcription factor EGR2 alleviates autoimmune uveitis via activation of GDF15 to modulate the retinal microglial phenotype. Proceedings of the National Academy of Sciences of the United States of America. 2024; 121: e2316161121. https://doi.org/10.1073/pnas.2316161121.

[18] Teruya S, Okamura T, Komai T, Inoue M, Iwasaki Y, Sumitomo S, *et al*. Egr2-independent, Klf1-mediated induction of PD-L1 in CD4$^+$ T cells. Scientific Reports. 2018; 8: 7021. https://doi.org/10.1038/s41598-018-25302-1.

[19] Jun JY, Ma Z, Pyla R, Segar L. Leptin treatment inhibits the progression of atherosclerosis by attenuating hypercholesterolemia in type 1 diabetic Ins2(+/Akita):apoE(-/-) mice. Atherosclerosis. 2012; 225: 341–347. https://doi.org/10.1016/j.atherosclerosis.2012.10.031.

[20] Kunkemoeller B, Chen K, Lockhart SM, Wang X, Rask-Madsen C. The transcriptional coregulator CITED2 suppresses expression of IRS-2 and impairs insulin signaling in endothelial cells. American Journal of Physiology. Endocrinology and Metabolism. 2021; 321: E252–E259. https://doi.org/10.1152/ajpendo.00435.2020.

[21] Suzuki R, Tobe K, Aoyama M, Inoue A, Sakamoto K, Yamauchi T, *et al*. Both insulin signaling defects in the liver and obesity contribute to insulin resistance and cause diabetes in Irs2(-/-) mice. The Journal of Biological Chemistry. 2004; 279: 25039–25049. https://doi.org/10.1074/jbc.M311956200.

[22] Ding F, Zheng P, Fang HT, Luo YY, Yan XY, Chen HJ, *et al*. Adipocyte-specific FAK deletion promotes pancreatic β-cell apoptosis via adipose inflammatory response to exacerbate diabetes mellitus. Clinical and Translational Medicine. 2024; 14: e1742. https://doi.org/10.1002/ctm2.1742.

[23] Wang J, Wang J, Yang L, Zhao C, Wu LN, Xu L, *et al*. CTCF-mediated chromatin looping in EGR2 regulation and SUZ12 recruitment critical for peripheral myelination and repair. Nature Communications. 2020; 11: 4133. https://doi.org/10.1038/s41467-020-17955-2.

[24] Kamran M, Liang J, Liu B, Li Y, Gao J, Keating A, *et al*. The Clusters of Transcription Factors NFATC2, STAT5, GATA2, AP1, RUNX1 and EGR2 Binding Sites at the Induced *Il13* Enhancers Mediate *Il13* Gene Transcription in Response to Antigenic Stimulation. Journal of Immunology (Baltimore, Md.: 1950). 2020; 205: 3311–3318. https://doi.org/10.4049/jimmunol.2000985.